



Performance and properties of K and TiO₂ based LNT catalysts

Laura Righini^a, Feng Gao^b, Luca Lietti^a, Janos Szanyi^b, Charles H.F. Peden^{b,*}

^a Dipartimento di Energia, Laboratory of Catalysis and Catalytic Processes and NEMAS, Centre of Excellence, Politecnico di Milano, Via La Masa 34, 20156 Milano, Italy

^b Institute for Integrated Catalysis, Pacific Northwest National Laboratory, Richland, WA 99354, USA

ARTICLE INFO

Article history:

Received 16 March 2015

Received in revised form 18 June 2015

Accepted 7 July 2015

Available online 18 July 2015

Keywords:

K/TiO₂

Potassium titanate

NSR

Thermal stability

NO_x adsorption

ABSTRACT

In this study, Pt-K/TiO₂ LNT catalysts having different K loadings (2, 5, 10, 15, 20 wt%) have been synthesized, characterized and tested, along with a Pt/K₂Ti₆O₁₃ reference material. The effects of K loading and thermal aging on NO_x storage performance have been addressed, and the formation/decomposition of stored NO_x species over Pt-free samples has been investigated by FT-IR, TPD and XRD techniques.

NO_x storage-reduction tests of Pt-K/TiO₂ catalysts indicate that 10 wt% K-loaded samples show the highest NO_x storage capacity, registered at 300 °C. Both the temperature at which the maximum NO_x storage capacity is attained and the NO_x uptake yields are a function of the K-loading.

A low K utilization in the NO_x storage has been observed. Especially at high K contents (K = 20 wt%) this result can be attributed, in part, to the low surface area of the support material, and to the depletion of the K storage phase via reaction between K and TiO₂. In fact XRD analyses demonstrate that K and TiO₂ react already during the catalyst synthesis calcination process by forming a "K₂Ti₆O₁₃-like" potassium titanate at temperatures as low as 550 °C. This reaction is promoted by increasing the K content and calcination temperatures. Activity, XRD and FT-IR measurements have demonstrated that poorly crystalline potassium titanates have appreciable storage properties. Upon aging treatments, K incorporates into the TiO₂ structure, leading to the formation of potassium titanates: this increase in the stability of K, on the other hand decreases the NO_x storage capacity. This raises questions concerning the capability of such systems to meet the durability requirements for vehicle emission control applications.

© 2015 Elsevier B.V. All rights reserved.

1. Introduction

Recent NO_x emission regulations in the automotive sector for lean burn and diesel fueled engines (currently US Tier 2 bin 5 and EURO 6) have led to increased interest in NO_x removal devices working under oxidizing environments [1–4]. Hence two after-treatment technologies have been developed: selective catalytic reduction (SCR) and lean NO_x traps (LNTs). The latter was introduced by Toyota in the '90s, and has been especially suitable for medium/light duty vehicles [5]. These NO_x trapping catalytic systems mainly consist of precious metals (Pt, Rh, Pd), to catalyze oxidation and reduction reactions, and alkali or alkaline-earth metals (including Ba or K) as the NO_x storage component on a high surface area support material, typically γ-Al₂O₃ or more sulfur and thermally stable Ce-Zr based supports [6]. The LNT concept is based on a catalytic cycle that alternates a lean phase under the normal

operation of the engine (1–2 min long), when NO_x are stored on the catalyst as nitrites or nitrates, with a short fuel-rich excursion of a few seconds to regenerate the catalyst by reducing the stored species into benign N₂.

Aiming at obtaining high NO_x conversions, many literature reports have dealt with the optimization of the catalyst formulation [7]. Traditional PtBa/γ-Al₂O₃ catalysts show high NO_x storage capacities in the low temperature region (200–400 °C) [8,9]. However, recent compliance issues with the introduction of lean burn gasoline engine technologies that operate at higher temperatures, including gasoline direct injection (GDI), has generated increasing interest in high temperature performance LNT catalysts [10]. While Ba is not suitable for these purposes due to the relatively low stability of Ba(NO₃)₂ and undesirable reactions between Ba and the Al₂O₃ support (forming BaAl₂O₄), K has shown high NO_x storage capacities above 400 °C attributed to its stronger basicity and mobility [9,11,12].

In particular, a few literature reports have demonstrated that K loading is a key factor in enhancing the NO_x stored species stability and high temperature performance for K-based LNTs on Al₂O₃ or

* Corresponding author. Fax: +1 509 371 6498.

E-mail address: Chuck.Peden@pnnl.gov (C.H.F. Peden).

MgAl_2O_4 supports [10,11,13]. Unfortunately, the volatile nature of the active K species, due to the much lower melting point (334°C) of KNO_3 , gives rise to technical challenges in avoiding loss of the active phase due to K volatilization, dissolution in water, and/or diffusion along with undesirable interactions with cordierite monolith supports [14,15]. Therefore, overcoming of K stability concerns is mandatory to its applicability in LNTs formulations.

These problems could perhaps be mitigated by using a catalyst support material able to minimize the mobility of K. TiO_2 seems to be a good candidate since K is known to strongly interact with it, readily forming potassium titanates, hence a possibly more stable LNT material. Moreover, TiO_2 has been already employed as an LNT support material due to its enhanced sulfur resistance [16,17]. On the other hand, potassium titanates, formed from a solid-state reaction between K and TiO_2 , could decrease the availability of K, leading to low NO_x storage capacities [18,19]. Thus, for example, TiO_2 has been applied together with Zr to avoid K– TiO_2 reaction [18]. Nevertheless, recent studies reported the synthesis and promising performance of potassium titanate-based LNT catalysts. For example Wang et al. [20] have recorded high-temperature NO_x storage capacity of thermally stable Pt/K₂Ti₂O₅ catalysts when compared to Pt–K/TiO₂ samples. These authors claimed that, even though K completely reacted with TiO_2 during a calcination process, K is still available to store NO_x via a reversible transformation from less to more K rich potassium titanate structures occurring upon switching from lean to rich conditions [21].

Naito and coworkers [22,23] and Zhang et al. [24] have shown high NO_x storage properties of Pt/KNO₃ and Pt/K₂CO₃ supported on K₂Ti₈O₁₇ potassium titanate nanobelts (prepared through a hydrothermal method). These results have been explained on the basis of K mobility in a K rich layer formed on the potassium titanate nanobelt surface [22]. However, the practical application of these systems is limited by the poor thermal stability, due to a collapse of the structure observed already at 500°C . Good activity of potassium titanate based materials has been reported in the case of an H₂-SCR process and in the simultaneous removal of NO_x and soot [25,26]. Although high NO_x adsorption capacities have been reported for potassium titanates, NO_x adsorption/reduction mechanisms over these catalysts need to be further verified and rationalized.

In this work, Pt–K/TiO₂ catalysts have been considered as potential candidates for NO_x storage; in particular, our primary aim was to investigate whether the TiO₂ supports are a good choice to stabilize K with reasonable NO_x storage efficiencies, and to what extent the reaction between K and TiO₂ can affect NO_x storage-reduction performance. Moreover, the behavior of potassium titanate reference materials (Pt/K₂Ti₆O₁₃ and Pt–K/K₂Ti₆O₁₃) have also been investigated, due to the fact that potassium titanates form upon calcination and aging of the Pt–K/TiO₂ catalysts. Accordingly, Pt–K/TiO₂ catalysts with different K loadings (2, 5, 10, 15, 20 wt%) have been prepared and characterized, and their catalytic activity in NO_x removal has been tested. The effect of K loading on trapped NO_x stability, NO_x storage capacity as well as catalyst structural properties has been addressed. Because thermal stability is known to be another important issue, LNTs with optimized K content were also used for studying the thermal aging effects on activity and catalyst structure.

Potassium titanate reference samples have also been prepared. These materials are prepared by many research groups through hydrothermal methods yielding high surface area materials [22,27]; these preparation methods have been employed in the present study as well. FT-IR experiments coupled with temperature-programmed desorption (TPD) measurements have been carried out for potassium titanate and K/TiO₂ samples with the aim to determine the nature and thermal stability of stored NO_x species.

2. Experimental

2.1. Catalyst preparation and aging treatments

Pt–K/TiO₂ catalysts have been prepared by the wetness impregnation method. The following procedure was utilized to ensure a high dispersion of the active elements and a high surface area of the final samples. Accordingly, the TiO₂ support as anatase (Hombikat UV 100), was dried at 80°C for 12 h. In order to incorporate Pt (1 wt%), the support powder has been contacted with a dilute solution of Pt(NH₃)₄(NO₃)₂ (Alfa Aesar), dried at RT for 12 h and at 80°C for 12 h, and finally calcined at 500°C 4 h in air. The Pt/TiO₂ sample was then impregnated with a solution containing K₂CO₃ (Alfa Aesar), as a precursor for K to obtain various loadings, i.e. 2, 5, 10, 15, 20 wt%. The K impregnated catalysts were then dried at RT for 12 h and at 80°C for 12 h, then calcined at 600°C for 4 h in air. Pt-free K/TiO₂ samples (K loadings of 2, 10, 20 wt%) were also prepared following the same procedure.

Potassium titanate materials were synthesized with hydrothermal methods to provide a catalyst with a high surface area by following procedures similar to ones reported in the literature [22,24,25,28–31]. The starting materials were 25 ml of 10 mol/l KOH solution (KOH from Sigma–Aldrich) and 0.75 g of P25 TiO₂ from Degussa. The preparation method consists of the addition of TiO₂ to the KOH solution under vigorous stirring in an autoclave for 30 min, then the autoclave was sealed and heated at 130°C for 4 days (operating pressure near 2.6 atm). After cooling to RT, the product was collected by alternating centrifugal filtration and careful washing with deionized water several times until a pH of ~ 9 was reached. The potassium titanate was dried at 80°C overnight under N₂ flow and then calcined at 600°C for 4 h. Potassium titanate-supported Pt and Pt–K10 catalysts were then prepared by wetness impregnation with protocols described above.

The samples were thermally aged by performing a calcination in air at 800°C for 4 h. The effect of the aging temperature has been studied in the case of Pt–K10/TiO₂ (K = 10 wt%) by aging the catalyst in air also at 650 and 700°C for 4 h.

2.2. Activity tests: NO_x storage capacity performance

NO_x storage capacities were measured by using a fixed bed quartz reactor (I.D. 95 mm), where 120 mg of catalyst powder was dispersed over a glass frit inside of the tube and then exposed to a flow of 400 ml/min (at 1 atm and 0°C), corresponding to a GHSV of 2×10^5 ml/g h. The exhaust gases were analyzed by a chemiluminescence NO_x analyzer (Thermo Electron, 42C). A typical NO_x storage capacity test consisted of a preliminary conditioning of the catalyst, carried out by performing 20 lean-rich cycles ($L/R = 50/10\text{s}$) to obtain a steady state working condition for the catalyst. Then a continuous lean flow was admitted to the reactor to evaluate the stored NO_x amounts. NO_x uptake ($\text{cm}^3/\text{g}_{\text{cat}}$) was defined as the amount of NO_x adsorbed until the outlet NO_x concentrations reached a 60 ppm value, normalized to the catalyst weight. Measurements were carried out from 550 to 250°C in 50°C steps. A flow of 150 ppm NO, 5% v/v O₂, 5% v/v CO₂, 5% v/v H₂O balanced by He was fed during the lean phase, while a flow of 4% v/v H₂, 5% v/v CO₂, 5% v/v H₂O balanced by He during the rich phase; H₂O was added to the gas flow via a syringe pump with other gas concentrations metered by mass-flow controllers. A 4-port valve manipulated via a Labview program via an electric actuator (Valco Instruments) was employed to accomplish the L/R switching.

2.3. Catalyst characterization

Temperature programmed desorption (TPD) of stored NO_x was carried out in the flow system described in the previous paragraph.

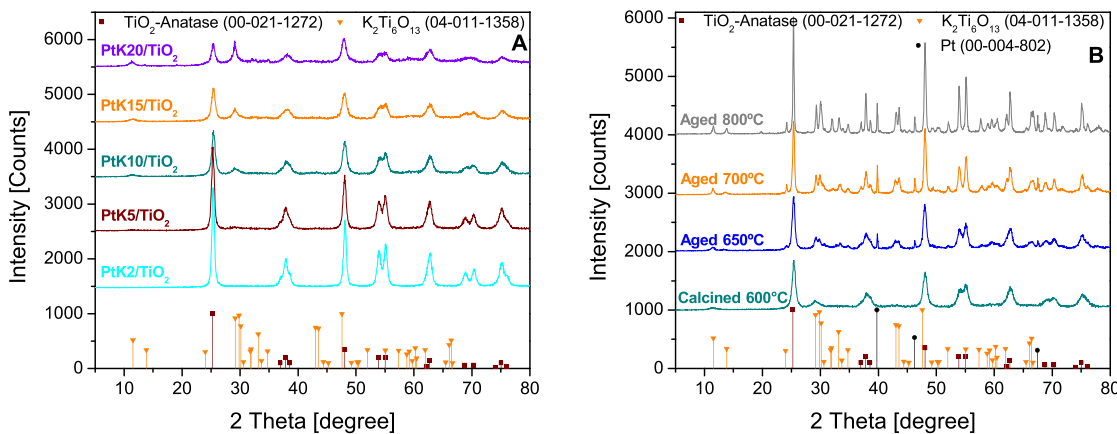


Fig. 1. Panel A: XRD analysis of fresh PtK_x/TiO₂ catalysts ($x = 2, 5, 10, 15, 20$ wt%), performed before reaction; Panel B: XRD analysis of a freshly calcined PtK10/TiO₂ catalyst, and after aging at 650, 700, 800 °C for 4 h.

NO_x was stored on 50 mg of catalyst powder by feeding 80 ml/min (at 1 atm and 0 °C) of 0.5% NO₂ in He (99.999% Purity, Matheson) at RT for 1 h to achieve saturation. After removal of physically adsorbed species through a He purge at RT for 2 h (200 ml/min at 1 atm and 0 °C), the catalyst temperature was linearly increased up to 600 °C at a rate of 5 °C/min, and then held at 600 °C for 2 h.

BET surface areas were measured with a Quantachrome Autosorb-6 analyzer, after sample outgassing at 150 °C overnight.

In situ XRD were collected on a Philips PANalytical X'Pert MPD system with a vertical θ - θ goniometer (220 mm radius). The X-ray source is a long-fine-focus and sealed ceramic X-ray tube with Cu anode that operates at 45 kV, 40 mA. The sample was placed on a sample stage (Anton Paar HTK 1200, temperature range 25–1000 °C) and heated in air flow from RT up to 800 °C. At each selected temperature, the XRD patterns (2θ from 10 to 50°) were obtained at a step size of 0.05° and a dwell time of 2 s. For evaluation of the effects of adsorbed NO₂, NO_x was first stored as in the case of the TPD experiments; i.e., loading 50 mg of catalytic powder in the flow reactor system by feeding 0.5% NO₂ in He at RT for 1 h, followed by a He purge at RT for 2 h (200 ml/min, at 1 atm and 0 °C).

Ex situ XRD were performed on a PANalytical X'Pert MPD system with a vertical θ - θ goniometer (190-mm radius). The X-ray source is a long-fine-focus and sealed ceramic X-ray tube with Cu anode, operating at 40 kV, 50 mA. The patterns were collected from 5 to 80° 2θ, using a 0.04° step size and 2 s per step. The analyses were carried out for samples before performing NO_x storage experiments, and after samples were removed from the flow reactor system. For the samples studied after FT-IR experiments, the dwell time was increased up to 24 s due to their small quantities.

Search of structural databases to identify the various phases present, and for calculations of particle size in the XRD measurements were performed using JADE 9 software and with Scherrer equation, respectively.

In-situ FTIR experiments were carried out in transmission mode, using a Bruker Vertex 80 spectrometer, working in the wavenumber range from 3900 to 400 cm⁻¹ with 4 cm⁻¹ resolution (average of 256 scans). The spectra were referenced to a background spectrum obtained from the clean sample (i.e., adsorbate-free). The powder samples were pressed onto a high-transmittance, fine tungsten mesh whose temperature was measured by an attached thermocouple. The sample on the tungsten mesh was heated resistively. The IR cell is attached to a pumping and gas handling system, and also to a mass spectrometer (UTI 100C). The mass spectrometer is connected to the IR cell through a leak valve that allows the monitoring of the gas phase in the IR cell during adsorption/reaction studies without significantly modifying the pressure in the cell. The FT-IR/TPD experiments consist of NO₂ adsorption at RT, followed

by evacuation of the reactant at RT and TPD of stored NO_x species up to 600 °C. The experiments were carried out in batch mode: precisely controlled amounts of NO₂ were introduced into the IR cell stepwise, and changes in the IR spectra were followed as a function of time and the amount of adsorbate introduced, as detailed elsewhere [32]. “NO₂-TPD cycling” will refer to the cyclic repetition of this experiment over each sample; i.e., when NO₂ adsorption and subsequent desorption have been repeated ~6 times.

Helium Ion Microscopy (HeIM) was performed using a Zeiss Orion microscope (Carl Zeiss, Oberkochen, Germany). Operating conditions were 30 keV and ~1.0 pA current, at a working distance of ~8 mm. Catalyst materials were placed on an aluminum stub with carbon tape and then placed into the HeIM chamber for observation.

3. Results and discussion

3.1. Characterization of K-based TiO₂- and potassium titanate-supported LNT catalysts

Fig. 1A presents the XRD data for freshly calcined Pt-K/TiO₂ catalysts (prior to performing the NO_x storage capacity tests) with K loading equal to 2, 5, 10, 15, 20 wt%. The diffraction pattern for the 2 wt% K sample clearly displays features related to the anatase support phase (PDF#00-021-1272). By comparing traces from the bottom to the top, it can be observed that the intensity of the anatase related peaks decreases as the K content increases and, in parallel starting from K loadings higher than 5 wt%, additional features appear. Rutile diffraction lines have not been detected in any of these samples.

The observed decrease of the area of anatase features could indicate that TiO₂ is reacting with K, leading to the formation of potassium titanates, in line with previous literature suggestions [18,19,33]. Accordingly, peaks are getting broader, possibly indicating that TiO₂ crystallites are getting smaller as they are consumed by the reaction, and/or the crystallites are developing strain, as a result of K incorporation. The observed additional peaks in Fig. 1A can be assigned to precursors of potassium titanates. The indication “precursors” has been used since the new “phases” are not completely crystalline. Fig. 1A also plots the major reference diffraction lines of the K₂Ti₆O₁₃ phase (PDF#04-011-1358), indicating that these additional features seem consistent with this phase. However, the observed patterns have broad peaks with intensity variations from the reference patterns, suggesting that a disordered phase has been obtained containing structural elements of K₂Ti₆O₁₃ and perhaps K₂Ti₈O₁₇. Notably, K₂Ti₆O₁₃ and K₂Ti₈O₁₇ are stoichiometric ordered members of mixed K₂O-TiO₂ phases

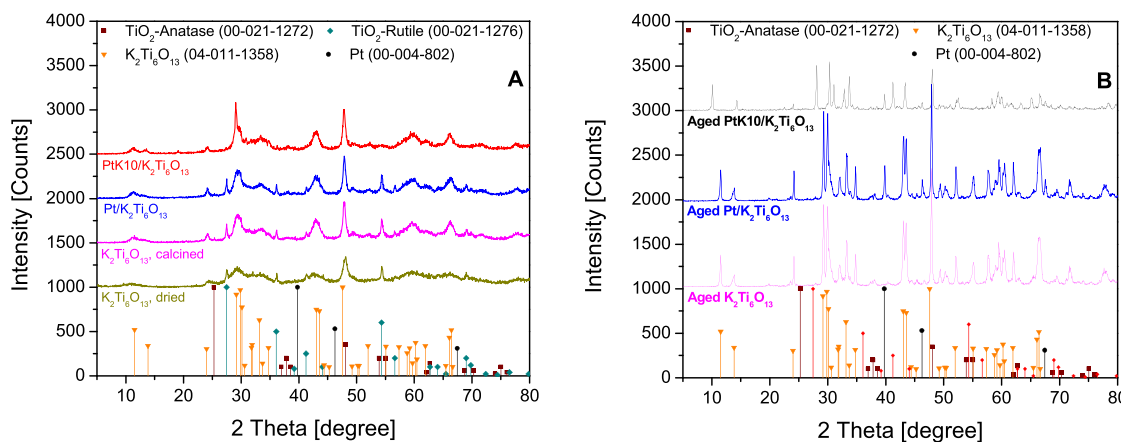


Fig. 2. Panel A: XRD analysis of dried and freshly calcined (at 600 °C) $\text{K}_2\text{Ti}_6\text{O}_{13}$, Pt/ $\text{K}_2\text{Ti}_6\text{O}_{13}$, and PtK10/ $\text{K}_2\text{Ti}_6\text{O}_{13}$ samples, performed before reaction; Panel B: XRD analysis of $\text{K}_2\text{Ti}_6\text{O}_{13}$, Pt/ $\text{K}_2\text{Ti}_6\text{O}_{13}$, PtK10/ $\text{K}_2\text{Ti}_6\text{O}_{13}$ samples aged at 800 °C for 4 h.

Table 1

Surface Area measurements of PtK10/TiO₂, K₂Ti₆O₁₃, Pt/K₂Ti₆O₁₃, PtK10/K₂Ti₆O₁₃ catalysts that were initially dried at 80 °C, calcined at 600 °C for 4 h, and aged at 800 °C for 4 h.

Samples		SA [m ² /g _{cat}]
PtK10/TiO ₂	Calcined 600 °C	57.6
PtK10/TiO ₂	Aged 650 °C	38.4
PtK10/TiO ₂	Aged 700 °C	14.3
PtK10/TiO ₂	Aged 800 °C	13.9
K ₂ Ti ₆ O ₁₃	Dried	240.2
K ₂ Ti ₆ O ₁₃	Calculated 600 °C	89.5
Pt/K ₂ Ti ₆ O ₁₃	Calculated 500 °C	66.2
PtK10/K ₂ Ti ₆ O ₁₃	Calculated 600 °C	45.8
K ₂ Ti ₆ O ₁₃	Aged 800 °C	12.5
Pt/K ₂ Ti ₆ O ₁₃	Aged 800 °C	11.8
PtK10/K ₂ Ti ₆ O ₁₃	Aged 800 °C	5.7

based on blocks of edge-sharing TiO₆ octahedra separated by planes where the octahedra share corners rather than edges. They differ only in the spacing between the corner-sharing planes and in the distribution of K within the edge-sharing blocks. However, by analyzing XRD patterns of aged samples (vide infra), it seems likely that the newly formed phase has a K₂Ti₆O₁₃ stoichiometry. Keeping in mind this fact, in the following discussion, “K₂Ti₆O₁₃-like” will refer to this initial poorly crystalline K₂O(x)-TiO₂(y) phase.

In summary, the XRD results indicate that: (i) no TiO₂ rutile is present; (ii) unlike the case for other supports, K is able to react with TiO₂, already during the calcination process, by forming a solid solution with a “K₂Ti₆O₁₃-like” stoichiometry, and the reaction is promoted by increasing the K content. Notably, by performing an in-situ XRD analysis at increasing calcination temperatures of K10/TiO₂ sample (temperature range: 25–600 °C, not shown here), potassium titanates formation has been evidenced by changes in the patterns at temperatures as low as 550 °C.

Since the Pt-K10/TiO₂ catalyst has shown the best initial performance for fresh (non-aged) catalysts (as described in the next section), and because material thermal stability is a crucial issue, this sample has been aged at 650, 700 and 800 °C for 4 h. The corresponding XRD analysis, performed before NO_x storage capacity measurements, are displayed in Fig. 1B, and compared with the one for the freshly calcined (at 600 °C) sample. The corresponding surface area (SA) measurements are summarized in Table 1. At increasing aging temperatures, the XRD patterns sharpen significantly for all of the present phases (i.e., TiO₂, Pt and potassium titanates), consistent with sintering during thermal treatments. Still, no diffraction lines attributable to rutile are present, highlighting that reaction between TiO₂ and K is favored with respect to

structure changes of the TiO₂ itself. The sharpness of the collected patterns allows a more in depth analysis of the diffraction peaks through JADE 9 software, and the obtained potassium titanate features display a best fit with the K₂Ti₆O₁₃ reference pattern. Note also a large SA decrease (up to almost four times at the highest calcination temperature, Table 1) as a result of these aging treatments.

Figs. 2A and B, along with Table 1 shows XRD and BET results for freshly calcined and aged potassium titanate-based samples. Features related to potassium titanates are present in the XRD pattern already for the freshly calcined materials (Fig. 2A). After calcination, sharper peaks due to potassium titanates are detected, indicating crystallization during the thermal treatment. A rutile related diffraction line at 27.46° (PDF #00-021-1276) is also present. Even after calcination at 600 °C, the synthesized material is poorly crystalline, as evidenced by the broadness of the diffraction peaks. Accordingly, the assignment of the peaks to K₂Ti₆O₁₃ or K₂Ti₈O₁₇ structure is not straightforward, as mentioned above. Many literature works have reported similar synthesis procedures and comparable XRD patterns, but different stoichiometries are sometimes identified [22,24,25,28–31].

While no obvious differences are evident by comparing traces of dried and calcined potassium titanates, a significant change of SA values from 240.2 to 89.5 m²/g_{cat} has been observed. The high SA value of the dried sample could indicate formation of a nanobelt structure, in line with results of Shen et al. [22] and Zhang et al. [24]. It is possible that the material composition has not changed during calcination (as verified by XRD and TGA-DSC analysis, in contrast to earlier reports [27]), but the calcination temperature (600 °C) may be high enough to destroy the nanobelt structure. Indeed, Shen et al. [22], by studying Pt-26KNO₃/K₂Ti₈O₁₇ samples, have shown collapse of the nanobelt structure upon high (>500 °C) temperature exposure.

No relevant changes are introduced in the diffraction patterns with Pt incorporation (Fig. 2A), although a decrease in the surface area has been observed. After K inclusion, rutile related peaks disappear, and also less intense diffraction lines for potassium titanates become detectable. It is likely that the added K has promoted formation of potassium titanates, as suggested by the pattern of the aged sample in Panel B (see below). Moreover, K addition strongly decreases the SA (roughly up to the half, Table 1).

Fig. 2B shows XRD analysis of the potassium titanate-based samples aged at 800 °C. Upon aging treatment, sharper and more intense peaks are evident, and the SA of the aged materials decreases significantly (Table 1), indicating support crystallization. The higher degree of crystallinity of the aged samples has facilitated the attribution of the “K₂Ti₆O₁₃” stoichiometry for the

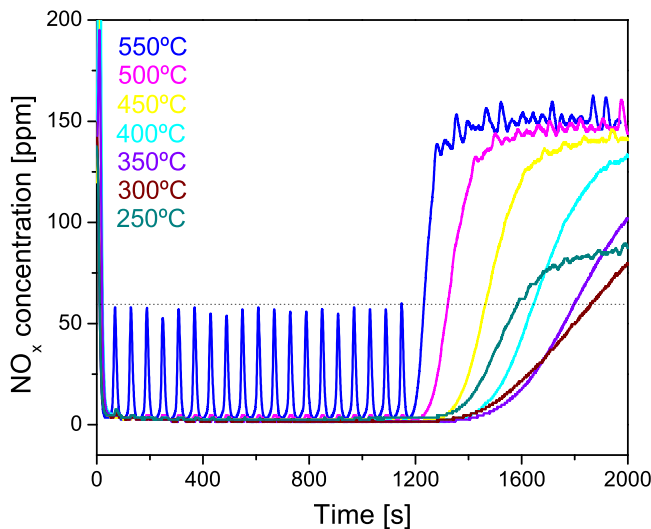


Fig. 3. NO_x concentrations at the different investigated temperatures (from 250 to 550 °C) during NO_x storage capacity measurements for a freshly calcined PtK10/TiO₂ catalyst. Lean phase: NO 150 ppm + O₂ 5% v/v + CO₂ 5% v/v + H₂O 5% v/v in He; rich phase: H₂ 4% v/v + CO₂ 5% v/v + H₂O 5% v/v in He.

obtained support. Hence, in the text this synthesized material will be referred to as K₂Ti₆O₁₃, although the phase is perhaps not fully crystalline. When Pt is also present, sharp diffraction peaks for Pt metal are also observed, indicating sintering of the precious metal upon aging treatment. For the case of the Pt-K10/K₂Ti₆O₁₃ catalyst sample, high temperature exposure leads to formation of potassium titanates with different stoichiometries and to much lower surface areas (SA = 5.7 m²/g_{cat}).

3.2. NO_x storage capacity measurements

3.2.1. NO_x storage over Pt-K/TiO₂

Fig. 3 depicts NO_x (NO + NO₂) concentrations registered during NO_x storage capacity measurements at all investigated temperatures for the case of a freshly calcined Pt-K10/TiO₂ catalyst (selected due to the best NO_x adsorption performances, vide infra). At 550 °C, NO_x concentrations gradually increase and decrease during lean/rich cycling of the catalyst. Later, upon continuous lean flow exposure, NO_x concentrations increase after a few seconds and finally reach input values corresponding to the fed amount. When NO_x concentrations reach 60 ppm, the total NO_x uptake is 0.55 cm³/g_{cat}. By decreasing the temperature, improved NO_x storage performance is obtained, as evidenced by the lower NO_x concentrations during cycling, and by the disappearance of the NO_x release at the lean/rich switch. During the final lean phase, a volcano-like dependence of complete NO_x uptake is observed, with a maximum uptake of 5.12 cm³/g_{cat} for reaction at 300 °C (Fig. 4A).

In Fig. 4A, NO_x uptake amounts (calculated as detailed in the experimental section) for Pt-K10/TiO₂ are compared with those obtained for freshly calcined Pt-K/TiO₂ with different K loading (K = 2, 5, 15, 20 wt%) over the 250 to 550 °C temperature range. For the case of the 2 wt% K-loaded catalyst, the maximum NO_x storage capacity is attained at 250 °C ($T_{NO_x\text{-max}}$), and the NO_x trapping performance decreases monotonically with increasing temperature. When K amounts are 5 and 10 wt%, the $T_{NO_x\text{-max}}$ corresponds to 300 °C, and it shifts to 350 and 400 °C by increasing the K loading up to 15 and 20 wt%, respectively. Concerning the NO_x uptake yields, values obtained above 400 °C are quite close for all samples with K ≥ 10 wt%, while the stored NO_x amounts are fairly similar for Pt-K/TiO₂ catalysts with 2 and 5 wt% K contents over the entire temperature range.

The main result of Fig. 4A is that, for each sample, an optimum performance temperature ($T_{NO_x\text{-max}}$) can be identified and this temperature shifts towards higher values for catalysts with increasing K loading. Also total NO_x uptake amounts are a function of the K content. These effects are similar to composition dependences previously observed for Pt-K/Al₂O₃ and Pt-K/MgAl₂O₄ catalysts [10,11,13]. Based on the present and prior results, it can be suggested that by increasing of K loadings: (i) formation of bulk-like KNO₃ is enhanced, explaining the higher thermal stability registered ($T_{NO_x\text{-max}}$ shift); (ii) the extent of coverage of Pt by K increases, consequently NO oxidation is suppressed and, in turn, the stored NO_x amounts ultimately decrease (maximum NO_x yields are observed at intermediate K contents). These points will be further discussed below.

Only for the case of Pt-K20/TiO₂ sample (in which TiO₂ does not seem to contribute to the NO_x storage, vide infra), the obtained stored NO_x amounts can be accurately normalized by the K content. It appears that the K utilization is very low (below 5%) over the entire investigated temperature range. However, for the cases of other support materials (Al₂O₃ and MgAl₂O₄), the K utilization is higher at this same K content (for example close to 40%) [13]. One reason could be that the TiO₂ support has a lower surface area compared to Al₂O₃ or MgAl₂O₄. This would then promote (probably already at lower K loadings, vide infra) formation of K bulk phases that are partially inaccessible to NO_x. Indeed, if a nominal coverage of K is calculated, it appears that a K monolayer can be obtained already for the case of 2 wt% K-loaded sample on TiO₂. Another explanation could be that the low support surface area could have increased the degree of Pt coverage by K. Finally, it is possible that part of K is depleted by the K-TiO₂ reaction, as indicated by XRD analysis of Fig. 1A.

Because the Pt-K10/TiO₂ catalyst leads to the highest overall NO_x storage, it was selected for further study of its thermal stability by carrying out aging treatments consisting of calcination at 650, 700 and 800 °C for 4 h in air. Fig. 4B displays the results of NO_x storage capacity tests for freshly calcined and aged Pt-K10/TiO₂. The catalyst is severely deactivated upon annealing, and it shows negligible storage properties after the 800 °C aging treatment. Moreover, increasing the aging times leads to a continuous decrease in the stored NO_x amounts (data not reported here).

Keeping in mind the corresponding XRD and BET analysis reported in Fig. 1B and Table 1, respectively, the decrease in the NO_x storage capacity upon aging can be ascribed either to Pt sintering, K dispersion, and/or to K phase loss resulting from the solid-state reaction between K and TiO₂. Decoupling the effects of Pt sintering and potassium titanates formation on the NO_x storage capacity has been carried out by comparing amounts of stored NO₂ at RT, collected by performing TPD experiments over freshly calcined Pt-K10/TiO₂ and K10/TiO₂, and on aged (800 °C, 4 h) K10/TiO₂. The results are reported in Table 2 in terms of NO_x stored amounts. The values are similar for freshly calcined Pt-K10/TiO₂ and K10/TiO₂ because the Pt oxidation function is not required when NO₂ is applied, demonstrating that the K10/TiO₂ sample is representative of the storage capacity of the Pt containing catalyst. A significantly lower NO₂ uptake (~9 times less) has been obtained for the aged K10/TiO₂ sample with respect to the freshly calcined Pt free one, highlighting that potassium titanates formation plays an important role in the deactivation of the storage properties.

Clearly, the K-TiO₂ reaction can affect the NO_x storage properties both in the freshly calcined and in the aged samples. As such, we also determined whether the presence of NO_x can affect the K-TiO₂ reaction and, thus, the morphology of the catalyst. Indeed, as pointed out previously for Al₂O₃-supported K LNT catalysts by Luo et al. [11], KNO₃ is present in a liquid-like state on the catalytic surface at fairly low temperatures. An in-situ XRD analysis of the Pt-K10/TiO₂ catalyst, with and without stored NO_x, has been

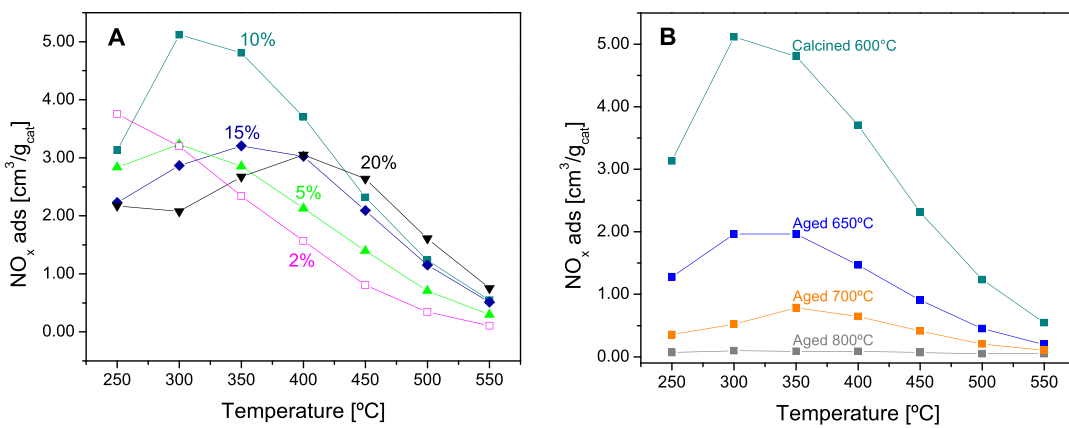


Fig. 4. Panel A: Stored NO_x amounts during NO_x storage capacity measurements for freshly calcined PtK_x/TiO₂ catalysts ($x = 2, 5, 10, 15, 20$ wt%); Panel B: NO_x stored amounts during NO_x storage measurements for a freshly calcined PtK10/TiO₂ catalyst, and after aging at 650, 700 and 800 °C for 4 h.

Table 2

Stored NO_x amounts, and NO₂/NO ratios obtained during TPD experiments for TiO₂, K_x/TiO₂ ($x = 2, 10, 20$ wt%), Pt1K10/TiO₂, K₂Ti₆O₁₃ samples calcined at 600 °C for 4 h, and a K10/TiO₂ sample aged at 800 °C for 4 h. NO_x adsorption: 0.5% v/v NO₂ in He at RT for 1 h, followed by a He purge for 1 h.

Sample	TiO ₂	K ₂ /TiO ₂	K10/TiO ₂	K20/TiO ₂	K ₂ Ti ₆ O ₁₃	K10/TiO ₂ aged	PtK10/TiO ₂
Stored NO _x [cm ³ /g _{cat}]	4.64	12.06	27.17	29.39	28.02	3.28	26.59
NO ₂ /NO	6.03	3.92	2.15	1.95	3.07	5.83	3.18

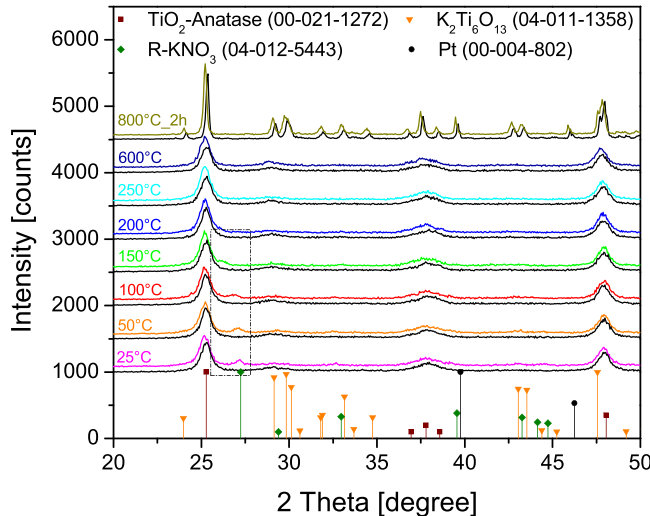


Fig. 5. In-situ XRD in air of PtK10/TiO₂ at different temperatures, collected before reaction (black lines) and after NO_x adsorption (colored lines). NO_x adsorption: 0.5% v/v NO₂ in He at RT for 1 h, followed by He purge for 1 h. (For interpretation of the references to color in this figure legend, the reader is referred to the web version of this article.)

carried out at increasing temperatures (from RT to 800 °C and then kept at 800 °C for 2 h). Some of the XRD patterns for the two series collected at different temperatures are reported in Fig. 5. The two series are essentially identical, indicating that, within the sensitivity of the XRD technique, NO_x does not seem to affect K-TiO₂ interactions. However, one notable difference has been observed by comparing the two groups of traces: the presence of an additional peak located at 27° (accompanied by much less intense ones at 32.68 and 39.23°) observed after NO_x storage. These are attributed to the formation of the rhombohedral KNO₃ phase (PDF#04-012-5443). In line with what has been reported by Luo et al. [11] for Al₂O₃-supported samples, the KNO₃ peaks disappear above 150 °C, indicating that the KNO₃ phase has melted, since its decomposition occurs at higher temperatures (namely at ~300 °C, as evaluated by TPD experiments for the Pt-K10/TiO₂ catalyst, data not shown).

To determine whether the aging treatment, along with formation/crystallization of potassium titanates, is changing the morphology of the sample, HeiM analysis (Fig. 6) was also performed on the 800 °C-aged catalyst and compared with one of the fresh samples. However, no significant changes in morphology were observed. As shown in Fig. 6, in the fresh sample sphere-like particles having 20–50 nm diameter are observed, while the 800 °C-aged catalyst appears as rectangular-like particles of higher size (~100 nm long), probably due to some primary particle agglomeration during the aging treatment.

3.2.2. NO_x storage on Pt/K₂Ti₆O₁₃

So far, the structure and activity of Pt-K/TiO₂ catalysts has been presented, with the results demonstrating that formation of potassium titanates readily occurs, and that this can affect the NO_x storage properties of the material. In fact, potassium titanates have been reported [20–24] to display useful NO_x storage properties themselves. As such, potassium titanates were studied with respect to their NO_x storage properties.

Fig. 7 shows the NO_x uptake for fresh Pt/K₂Ti₆O₁₃ and Pt-K10/K₂Ti₆O₁₃ materials, along with those of Pt-K10/TiO₂ for comparison purposes. It can be seen that NO_x uptake values for the Pt/K₂Ti₆O₁₃ sample increases by roughly 22% with respect to the Pt-K10/TiO₂ one without changing T_{NO_x-max}. Both catalysts experience severe loss of NO_x storage performance after the aging treatment at 800 °C and only negligible amounts of NO_x is adsorbed; for example, while Pt/K₂Ti₆O₁₃ has a maximum stored NO_x amount of 0.5 cm³/g_{cat} at 450 °C (data not shown), the Pt-K10/TiO₂ catalyst has trapped a negligible amount of NO_x, as illustrated in Fig. 4B.

To understand the nature of the storage sites in these materials, we recall recent literature contributions for comparison purposes. Wang et al. [20,21], by comparing activity of Pt-K/TiO₂ (K/Ti = 0.5, 1) and Pt/K₂Ti₂O₅ catalysts, have reported much higher thermal stability of stored NO_x for the potassium titanate-based samples. This result was explained by a reversible transformation from less to more K rich potassium titanates structures (namely, K₂Ti₂O₅ with K₂Ti₆O₁₃) occurring upon switching from lean to rich conditions. This mechanism, involving a K rich layer obtained on the potassium titanate nanobelt support, was used by Shen et al. [22] to rationalize

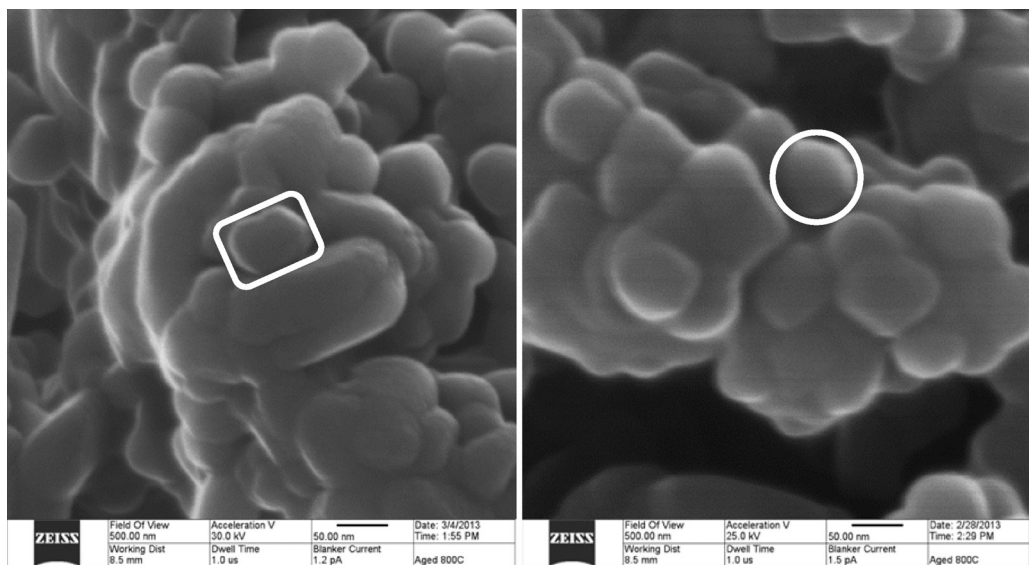


Fig. 6. HeIM images of freshly calcined and aged (at 800 °C) PtK10/TiO₂ catalysts before reaction.

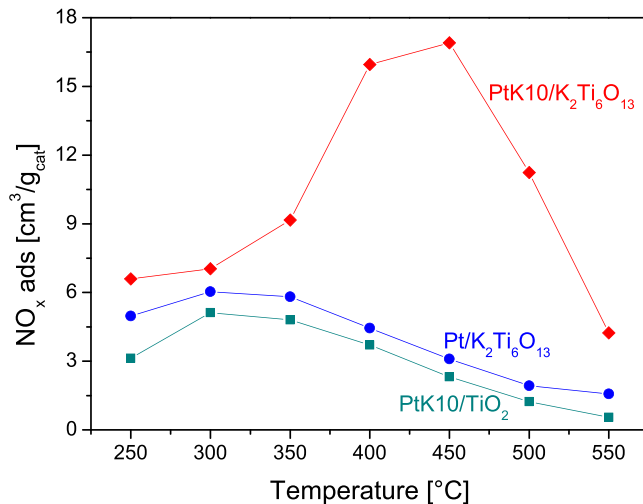


Fig. 7. Comparison of NO_x stored amounts for freshly calcined PtK10/TiO₂, Pt/K₂Ti₆O₁₃, and PtK10/K₂Ti₆O₁₃ samples. NO_x storage reaction conditions: lean phase: NO 150 ppm + O₂ 5% v/v + CO₂ 5% v/v + H₂O 5% v/v in He; rich phase: H₂ 4% v/v + CO₂ 5% v/v + H₂O 5% v/v in He.

the high NO_x storage performance for Pt-K/K₂Ti₈O₁₇ catalysts, with respect to more commonly studied Pt-K/Al₂O₃ LNT systems.

Our data do not show such high stored NO_x thermal stabilities described by Wang et al. [20]. This discrepancy may perhaps be due to the different stoichiometries of the potassium titanates used, and/or different amounts of K and Pt loadings utilized during the synthesis. Note, however, that a comparison of the results presented by Shen et al. [22], it appears that the data of Fig. 7 are consistent with this latter prior work; notably, the authors report that a Pt/K₂Ti₈O₁₇ material does not display much enhanced NO_x storage capacity. In particular, a quite low K utilization has been calculated (9%), and NO_x storage is significantly promoted only with the addition of extra K.

In summary, NO_x storage capacity data for fresh and aged samples discussed here and corresponding XRD analysis reported above (Figs. 1 and 2), as well as a comparison of literature data suggests that optimum storage phases are K₂O or at least a poorly crystalline K_xTi_yO_z surface phase, in which the K sites are exposed to the external surface of the material. In this model, K is linked to Ti

in the surface phase, thereby reducing K mobility and decreasing its availability to store NO_x, in line with previous literature suggestions [18,19,34]. Then, the development of more fully crystalline potassium titanate phase upon aging leads to the reduction of NO_x storage performance. We have found no evidence for the previously proposed [20,21] structure change mechanism.

3.2.3. NO_x storage on Pt-K/K₂Ti₆O₁₃

Results discussed so far likely suggest that catalyst deactivation upon heating is related to a reaction between K and TiO₂ leading to the formation of highly crystalline potassium titanates. Accordingly, we asked the question whether the introduction of additional K could lead to higher stored NO_x amounts and more stable catalysts. In particular, we reasoned that a potassium titanate support might prevent further reaction of K and the corresponding loss of its NO_x storage properties. Therefore NO_x storage capacity tests for a Pt-K10/K₂Ti₆O₁₃ catalyst were carried out and compared with those for Pt-K10/TiO₂ and Pt/K₂Ti₆O₁₃ catalysts in Fig. 7. The results demonstrate that, upon further addition of K, stored NO_x amounts dramatically increase, and the T_{NO_x-max} is now ~450 °C. As such, further studies of these titanate-supported K-based LNT catalysts are warranted, but are beyond the scope of the present work. We do note, however, that these promising results must be tempered by the fact that the aging of the Pt-K10/K₂Ti₆O₁₃ catalyst at 800 °C resulted in almost complete loss of NO_x storage capacity (data not shown). On this basis, we suggest that the problem of K mobility, that can even be enhanced by the presence of NO_x, may prevent practical application.

3.3. Surface and gas phase characterization by FT-IR and TPD analysis of stored NO_x stability, catalyst stability and K-TiO₂-NO_x interaction

The results so far reported have identified a number of issues: (i) the relationship between the K loading, the stability of the stored NO_x and the NO_x uptake; (ii) the role of potassium titanates as a storage material; (iii) the role and the importance of the K-TiO₂ reaction in affecting the NO_x storage capacity. To clarify such aspects, the nature and stability of stored NO_x species over K/TiO₂ (with K content equal to 0, 2, 10 and 20 wt%) and K₂Ti₆O₁₃ samples have been studied by FT-IR analysis of adsorbed species upon exposure to NO₂ at RT, subsequent NO_x TPD measurements,

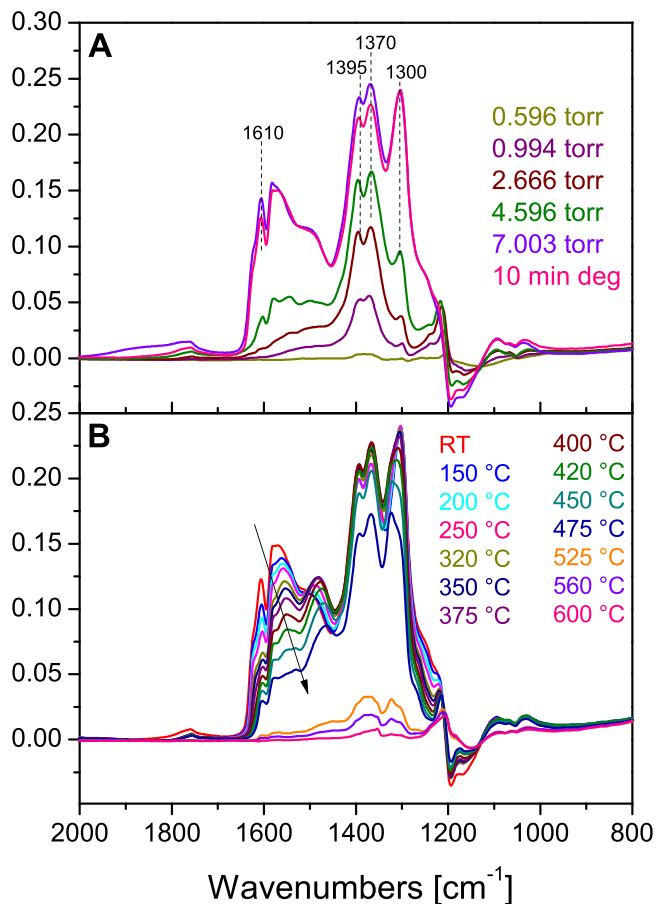


Fig. 8. FT-IR spectra for a K10/TiO₂ sample collected upon NO₂ dosing up to saturation and subsequent evacuation at RT (Panel A), and during heating in subsequent temperature-programmed desorption (Panel B).

and XRD. To mimic the conditions after lean/rich cycling, room temperature NO₂ adsorption and desorption were carried out several times, and the results shown here are after 5 adsorption/desorption cycles followed by a 6th NO₂ adsorption step.

FT-IR spectra for increasing NO₂ pressures over the K10/TiO₂ sample are displayed in Fig. 8A. These spectra appear quite complex in view of the many features present. In particular, adsorption of NO_x species has been evidenced in the 1800–1000 cm⁻¹ region, in which the three most intense bands are at 1395, 1370 and 1300 cm⁻¹. These peaks grow with NO₂ concentration accompanied by bands in two additional regions: 1650–1500 cm⁻¹ and 1250–1200 cm⁻¹. Above ca 2.7 Torr, the intensities of the 1650–1500 cm⁻¹ features increase at a higher rate with respect to the ones between 1400 and 1300 cm⁻¹, while those between 1250 and 1200 cm⁻¹ seem already saturated at this point. All of these FT-IR features remain quite stable under subsequent evacuation (10 min degassing).

By comparing spectra related to NO₂ adsorption over TiO₂ (vide infra, Fig. 9) with the one collected at the end of the adsorption in Panel A, despite considerable overlap of the peaks, a qualitative separation of the main adsorbed species to either TiO₂ or the K storage phase can be made. In particular, we attribute the spectral contribution of TiO₂ after NO_x storage to the features at higher (1630–1610 cm⁻¹) frequencies, as will also be confirmed by TPD experiments (vide infra).

Focusing on the nitrate species formed on K sites, previous studies of NO₂ adsorption over K and Pt-K/Al₂O₃ supported catalysts have identified formation of chelating bidentate nitrates (ν_{asym} modes 1309 cm⁻¹ along with ν_{sym} ones at 1040 and $\nu(\text{N}=\text{O})$

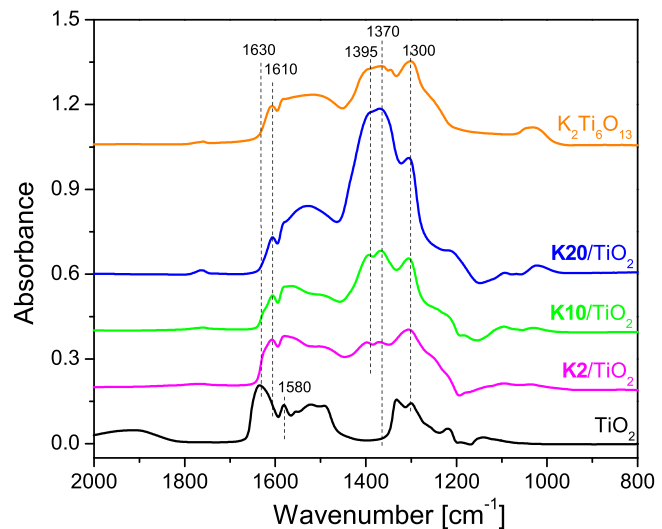


Fig. 9. Comparison of FT-IR spectra collected upon NO₂ dosing up to saturation and subsequent evacuation at RT for the freshly calcined Pt-free samples studied here (TiO₂, K₂/TiO₂, K₁₀/TiO₂, K₂₀/TiO₂, K₂Ti₆O₁₃).

1570–1530 cm⁻¹) and ionic nitrates (ν_{asym} modes at 1395 cm⁻¹ and 1370 cm⁻¹; ν_{sym} modes at 1040–1030 cm⁻¹) [10,13,35–37]. By analyzing the spectra collected after evacuation in Panel A of Fig. 8, it is clear that both of these types of K-nitrates have formed in the K₁₀/TiO₂ sample, and, as suggested by previous literature [13,38], these can be attributed to bulk-like (ionic) and surface (bidentate) K-nitrates, respectively. Indeed, ionic nitrates are evidenced by two of the three main features (at 1395 and 1370 cm⁻¹), in line also with TPD results (vide infra). The third main feature at 1300 cm⁻¹ can be related to surface KNO₃ species, likely chelating bidentate nitrates, despite a possible small contribution to this peak from nitrates stored on TiO₂.

In order to identify which are the most stable NO_x species, evolution of FT-IR spectra during a temperature ramp following the NO₂ storage on K₁₀/TiO₂ has been obtained and shown in Panel B of Fig. 8. At the initial stage of the temperature rise, a decrease in the intensity of only bands belonging to high frequency (above 1500 cm⁻¹) and 1250–1220 cm⁻¹ regions is observed, with also a small decrease of the band at 1300 cm⁻¹ and a parallel increase in the intensity of the band centered at 1480 cm⁻¹. Very minor increases in peak intensities at 1030, 1395 and 1370 cm⁻¹ up to 400 °C are also evident. Some of these changes, notably the small decreasing peak intensities that approximately parallel small increases in other peaks, suggest a transformation between different types of nitrate species. Above this temperature, all FT-IR features decrease in intensity as the various nitrate species decompose, and after 2 h at 600 °C the sample is completely regenerated. Based on the persistence of the 1370 and 1390 cm⁻¹ bands, especially at lower temperatures, ionic (bulk-like) K-nitrates seem to be the most stable adsorbed NO_x species.

Fig. 9 reports the spectra collected at the end of the adsorption phase (after NO₂ evacuation) for all samples, showing the effect of K loading on the distribution of the various types of nitrate species adsorbed, as well as which species are present on the K₂Ti₆O₁₃ support. In the spectrum from the TiO₂ sample in Fig. 9, ν_{asym} modes at high wavenumbers (e.g., peaks at 1630, 1580, 1550–1490 cm⁻¹) along with ν_{sym} modes at low wavenumbers (registered at 1330, 1300, 1250–1220 and just below 1150 cm⁻¹) are all assignable to nitrate species adsorbed on TiO₂, based on prior literature [39–43].

New features in the Fig. 9 spectra, due to NO_x stored on the K storage phase are clearly evident, as are their intensity variations with increasing K content. Notable in these spectra is that,

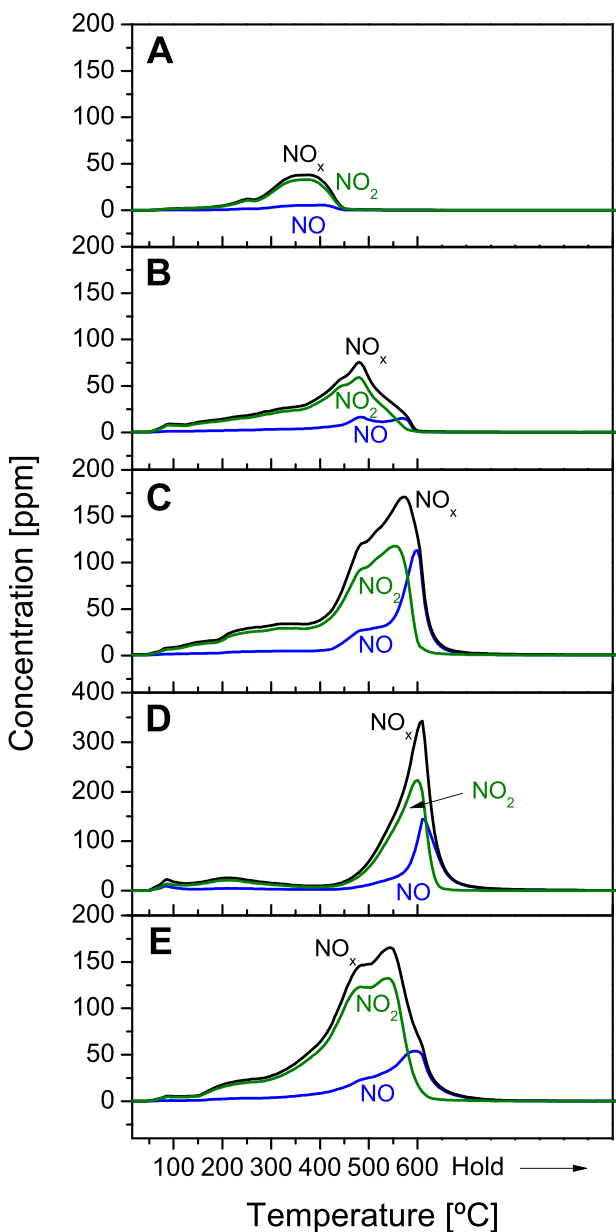


Fig. 10. NO, NO₂ and NO_x concentrations collected during the temperature-programmed desorption measurements for TiO₂ (Panel A), K2/TiO₂ (Panel B), K10/TiO₂ (Panel C), K20/TiO₂ (Panel D) and K₂Ti₆O₁₃ (Panel E) samples (NO_x adsorption: 0.5% v/v NO₂ in He at RT for 1 h, followed by He purge for 1 h).

at low K content (2 wt%), the intensities of ionic nitrate-related bands (centered at 1395 and 1370 cm⁻¹) are significantly lower than the features at 1300 between 1610 and 1550 cm⁻¹. By increasing K loading, the relative intensities of ionic to other nitrate species increases, indicating that NO_x is stored primarily as ionic (bulk-like) K-nitrates at high loadings.

The shape of the K20/TiO₂ sample spectrum seems different from the ones with lower K levels because the TiO₂ contribution to the NO_x storage was likely less important, as also confirmed by TPD analysis (see Fig. 10). Moreover, the FT-IR features have become broader at high K content, evidencing phase heterogeneity, as also suggested by XRD analysis (vide infra, Fig. 12).

Finally, Fig. 9 displays the FT-IR spectrum obtained for NO_x adsorption on the potassium titanate sample. A primary result is that the material described shows NO_x storage properties. By analyzing the relative intensities of the main features, it appears that

the ratio between ionic and other nitrates is similar to the K10/TiO₂ sample, and an additional feature at 1345 cm⁻¹ is registered. Also notable is that peaks obtained for the potassium nitrate sample are even broader than the ones for K20/TiO₂.

In order to confirm observed trends, further investigations of the K morphology and of thermal stability of adsorbed NO_x species formed on K/TiO₂ (K = 2, 10, 20 wt%), K₂Ti₆O₁₃ and TiO₂ (as a reference) materials were performed by carefully analyzing NO and NO₂ evolution during TPD experiments in the flow reactor system. TPD curves of all studied samples are illustrated in Fig. 10, Panels A–E. Similar to the FT-IR experiments, NO₂ has been adsorbed at RT up to saturation. Table 2 summarizes calculated NO_x adsorbed amounts and NO₂/NO ratios of the desorption products.

Panel A of Fig. 10 reports NO and NO₂ traces evolved from decomposition of stored NO_x on TiO₂. Initially desorption of weakly adsorbed species is registered; above 265 °C the decomposition leads to NO₂ as the main product, accompanied by very small amounts of NO evolving with two maxima. The TiO₂ support has very weak storage capacity (4.64 cm³/g_{cat}, Table 2).

Fig. 10B displays TPD results for the K2/TiO₂ sample. With small addition of K (2 wt%), initial NO₂ evolution is observed, resembling the desorption traces of the TiO₂ sample, coming from weakly adsorbed species. Above ca. 350 °C NO₂ evolves with high rates, with the NO desorption occurring later in two features (respectively, maxima located at 485 and 570 °C). The storage, relative to TiO₂, is enhanced after addition of 2 wt% K (NO_x uptake is calculated 12.06 cm³/g_{cat}), while desorbed NO amounts are still much lower than NO₂. By comparing traces of Panel B–D it can be noticed that increasing K loading leads to a shift of the decomposition onset temperature to higher values, increases in the NO_x stored amounts, and decreases in the NO₂/NO ratios (Table 2) of the decomposition products. For the case of K20/TiO₂ (Panel D), desorption features related to the TiO₂ contribution are negligible. In line with FT-IR data of Fig. 9, it can be suggested that, in this case, there are sufficient amounts of K in the sample to prevent NO_x storage on TiO₂, and that the formation of the bulk-like K-nitrate phase predominates, explaining the high temperature characteristics. Indeed, the result appears very similar to that obtained for Ba/Al₂O₃ samples [38]: TPD results collected under the same conditions for BaO/Al₂O₃ samples have shown desorption of NO₂ at low temperatures and later that of NO, which have been assigned to the decomposition of surface (chelating bidentates) and bulk (ionic) barium nitrate species, respectively [38]. Indeed with increasing Ba loading, the higher temperature evolution of NO becomes dominant, due to the formation of three dimensional BaO clusters. Additionally, TPD trends as a function of K loading presented here are in good agreement with those for K/Al₂O₃ and K/MgAl₂O₄ LNTs [10,13]. Accordingly, results for TiO₂-based samples suggest that, at low K loadings, the K-support interaction leads to highly dispersed "surface nitrates", while at high loadings bulk-like KNO₃ forms. However, the low surface area of the TiO₂ support used here promotes bulk K phase formation already at fairly low K loadings and the increase of K content further promoted formation of this phase.

Finally, the TPD experiment for the K₂Ti₆O₁₃ sample again confirms that this material has NO_x storage capacity, in line with the FT-IR and NO_x storage capacity data. Interestingly, as with the FT-IR data in Fig. 9, the TPD curves for the K₂Ti₆O₁₃ sample are quite similar to the ones for K10/TiO₂ both in terms of temperatures at which maximum NO and NO₂ concentrations are attained and the NO₂/NO ratios, although peaks are somewhat broader for K₂Ti₆O₁₃. The corresponding NO_x stored amount is close to values of the 10 and 20 K wt% samples.

XRD patterns of freshly calcined and used (for TPD) samples have also been collected. These show the formation of crystalline potassium titanates during the TPD experiments with an extent proportional to the K content. To better enlighten these aspects,

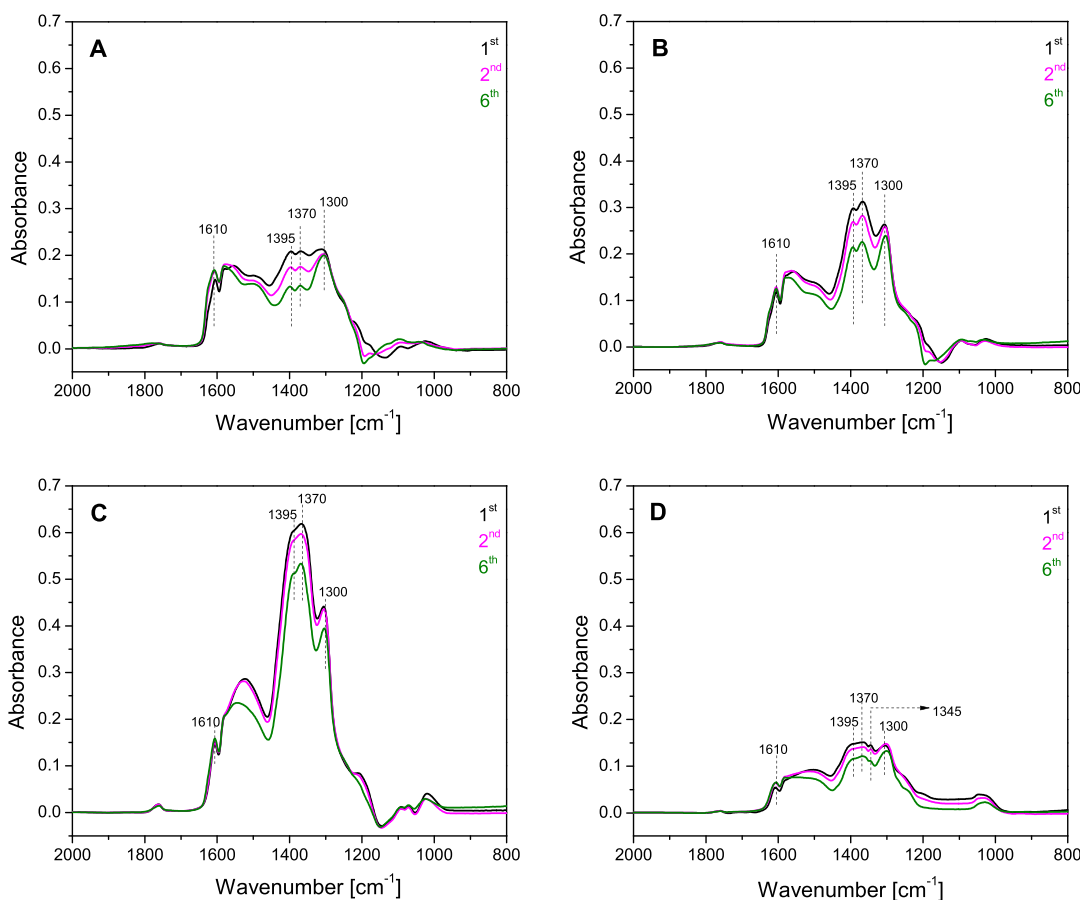


Fig. 11. FT-IR spectra collected after NO₂ dosing up to saturation and subsequent evacuation at RT for K2/TiO₂ (Panel A), K10/TiO₂ (Panel B), K20/TiO₂ (Panel C), and K₂Ti₆O₁₃ (panel D) samples. Spectra displayed were obtained after the 1st, 2nd and 6th NO₂-TPD experiments.

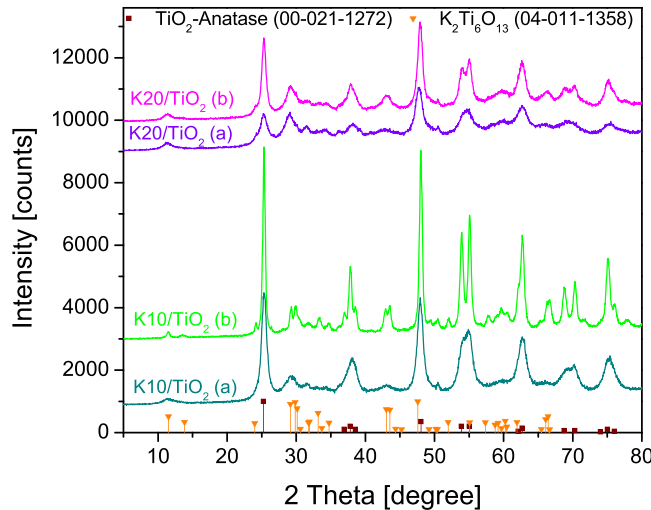


Fig. 12. XRD patterns of K10/TiO₂ and K20/TiO₂ samples before (a) and after (b) NO₂-TPD cycling.

additional NO_x adsorption/desorption studies have been carried out. These experiments consisted of NO₂ adsorption at RT followed by annealing to remove adsorbed NO_x species. These procedures were repeated at least 6 times for each sample. Fig. 11, Panels A–D shows the spectra recorded at the end of the NO₂ adsorption after evacuation, recorded after the 1st, 2nd and 6th NO₂ adsorption processes for the K_x/TiO₂ ($x=2, 10, 20$ wt%) and K₂Ti₆O₁₃ samples. As already discussed, many FT-IR features are observed in the spec-

tra making it difficult to separate individual contributions from each adsorbed NO_x species, hence only a qualitative approximate analysis will be provided here.

Panel A of Fig. 11 displays the result for the K2/TiO₂ catalyst. By cycling the catalyst, a decrease in the intensities of some bands is observed, especially ionic nitrate-related features (1395, 1370 cm⁻¹), while the peak at 1300 cm⁻¹ is stable and the 1610 cm⁻¹ peak slightly increases. At higher K contents (panels B and C), the decrease of FT-IR intensities is more extensive, involving almost all of the present features except for the one at 1610 cm⁻¹. Results for the K₂Ti₆O₁₃ sample (panel D) are qualitatively similar to those obtained for K/TiO₂ at higher K loadings. In all cases, the intensity loss for bands related to ionic nitrates (1395 and 1370 cm⁻¹) is especially evident. By focusing on the intensity of the band centered at 1395 cm⁻¹, it seems that the 2 wt% K-loaded sample shows the most significant decrease in the intensity of the bands. On the other hand, NO₂-TPD cycling carried out over TiO₂ (not shown here) indicates that TiO₂ is stable upon interaction with NO_x and subsequent NO_x desorption treatments.

The decrease in the intensities of some peaks observed for K containing samples suggests that no stable performance can be obtained in the presence of K. Indeed, we suggest that it is possible that K loss has occurred during NO₂ adsorption/desorption cycling. Notably, such a loss of the K-storage phase from the LNT catalyst could be a result of the quite low KNO₃ melting temperature, which is below that of KNO₃ decomposition [11]. Furthermore, as already noted, we have observed the formation of potassium titanates during the NO₂ TPD. On the other hand, the lowest decrease in NO_x uptake with cycling has been observed for the K₂Ti₆O₁₃ sample, where K and TiO₂ have already reacted.

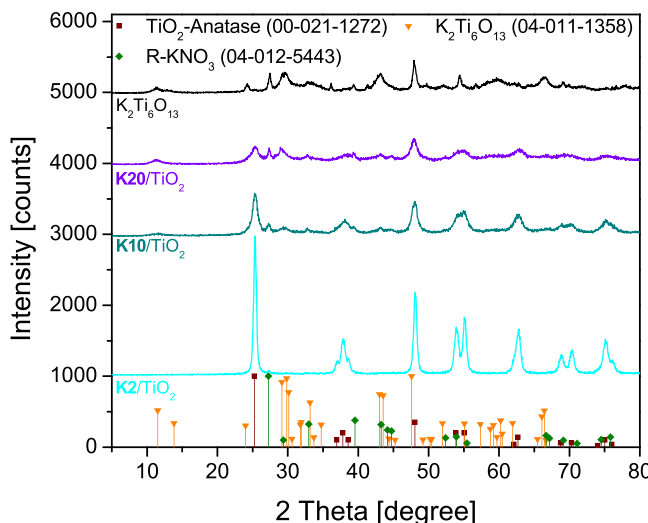


Fig. 13. XRD patterns for K_x/TiO_2 ($x=2,10, 20$ wt%) and $K_2Ti_6O_{13}$ samples with stored NO_x (NO_x adsorption: 0.5% v/v NO_2 in He at RT for 1 h, followed by He purge for 1 h).

In order to further probe the structure changes occurring during NO_2 -TPD cycling, and how these might affect the NO_x uptake performance, XRD analysis of used $K10/TiO_2$ and $K20/TiO_2$ catalysts were carried out after removing the samples from the supporting grid used to perform the FT-IR experiments. The results are illustrated and compared with the freshly calcined ones in Fig. 12, where it can be seen that, in both cases, sharper and more intense peaks related to anatase and potassium titanates phases are observed after NO_2 -TPD cycling. Moreover, less intense potassium titanate diffraction lines become detectable. These changes demonstrate that additional potassium titanates formation and/or crystallization has occurred during NO_2 -TPD cycling. Apparently, despite the fact that the material has been calcined at $600^\circ C$ for 4 h, K continues to react with TiO_2 . In fact, evidence for this reaction was also obtained when the annealing was stopped at a lower temperature of $550^\circ C$, but maintaining the sample at this temperature for a longer time to ensure the NO_x removal; also in this case, a decrease in the NO_x storage property was observed in the FT-IR data (not shown). Accordingly, the formation or crystallization of potassium titanates can likely explain, at least in part, the decrease in NO_x storage capacity observed in the FT-IR experiments (Fig. 11).

Finally, the stored NO_x species have been characterized with XRD. For this purpose, NO_2 was adsorbed on the catalysts in the flow reactor system following the same procedures as used in the TPD experiments. After the He purge, the sample was taken out of the reactor, and an ex-situ XRD analysis was performed. As shown in Fig. 13, patterns have been recorded for K/TiO_2 (K = 2, 10, 20 wt%) and $K_2Ti_6O_{13}$ powders. Concerning the K/TiO_2 traces, a feature located at $2\theta=27^\circ$ (accompanied by less intense ones at 32.68 and 39.23°) is readily detected, arising from the presence of the rhombohedral KNO_3 phase (PDF#04-012-5443). Although this feature is barely detectable in the case of $K2/TiO_2$, its intensity clearly increases at higher K loadings. Using the peak centered at 27° , a Scherrer equation estimate of crystallite sizes yields values of 19 to 25 nm for the K10 and K20 wt% samples, respectively. For the case of the $K_2Ti_6O_{13}$ sample, nitrates formation is even more evident from the peak corresponding to $2\theta=39.5^\circ$, despite the fact that it slightly overlaps with the potassium titanate-related feature. These results demonstrate that KNO_3 has formed upon NO_2 exposure at RT, and that a bulk-like KNO_3 phase is obtained already at low K loadings, while higher K content yields an increase in the amount of this phase.

4. Concluding remarks

In this work Pt-K/ TiO_2 (K: 2, 5, 10, 15, 20 wt%) catalysts have been synthesized, characterized and tested to determine whether the selected support can provide K-based LNT catalysts with stable NO_x storage performance. The effect of K loading and thermal stability issues have been addressed by studying formation and stability of stored NO_x species over corresponding Pt-free samples. Since a potassium titanate phase was formed in these samples, Pt- $K_2Ti_6O_{13}$ and Pt-K10/ $K_2Ti_6O_{13}$ reference materials have also been prepared.

Activity tests for the Pt-K/ TiO_2 catalysts show that the maximum NO_x uptake temperature ($T_{NO_x-\max}$) increases with the K content, and that NO_x uptake yields are maximized for the 10 wt% K-loaded-catalysts (at $300^\circ C$). In parallel, by storing NO_2 on the K/ TiO_2 (K: 2, 10, 20 wt%) samples, combined use of FT-IR and TPD techniques reveals that formation of ionic nitrate species is enhanced at increasing K loadings, although these species are already present even at low K contents in small amounts. Their presence has been correlated with the formation of a bulk-like K storage phase, explaining enhanced NO_x thermal stability at higher K loadings. This composition dependence is a peculiarity of the K storage compound, as already highlighted for Al_2O_3 - and $MgAl_2O_4$ -supported Pt-K catalysts [10,11,13]. On the basis of this prior work, the shift of the $T_{NO_x-\max}$ in our data may be explained by the promoting effect of the K content on the formation of the bulk-like storage phase, while a detrimental effect of still larger K amounts on NO_x uptake yields may be due to the encapsulation of Pt by K. On the other hand, a rather low K utilization has been obtained for the Pt-K/ TiO_2 catalysts, in contrast to the Al_2O_3 - and $MgAl_2O_4$ -supported catalysts. This result may be explained by the low surface area of the TiO_2 support that can favor Pt encapsulation by K and can promote formation of the bulk-like KNO_3 phase already at low K contents, as also evidenced by XRD, FT-IR and TPD data. Furthermore, the low K utilization is likely due, at least in part, to the depletion of the K storage phase via a solid-state reaction between K and TiO_2 .

According to NO_x storage capacity and FT-IR data, potassium titanates have storage properties. However, reactivity measurements and TPD experiments for freshly calcined and aged catalysts demonstrate that potassium titanate formation/crystallization at high temperatures decreases NO_x stored amounts, thereby apparently lowering the K available for NO_x storage. Moreover, cyclically performing NO_2 -TPD experiments shows that K/TiO_2 and $K_2Ti_6O_{13}$ materials do not display stable NO_x storage performance, likely due to potassium titanates formation/crystallization and K loss. Hence, all results consistently demonstrate that, while the reaction between K and TiO_2 can lead to a positive decrease in the mobility of K, the formation of potassium titanates reduces the number of K sites. Our results provide no evidence for a structure change mechanism between less/rich K potassium titanates structures, as proposed in prior literature reports [22,24].

Finally, a primary conclusion of the present work is that issues of K mobility and reactivity with support materials may well be a fatal flaw for these candidate high-temperature LNT catalysts, at least for vehicle applications where temperatures in excess of $550^\circ C$ are expected during periodic soot filter regeneration and sulfur removal processes.

Acknowledgements

Financial support was provided by the U.S. Department of Energy (DOE), Office of Energy Efficiency and Renewable Energy, Vehicle Technologies Program. The authors gratefully acknowledge Dr. Mark Bowden for analysis of the XRD data, Dr. Tamas

Varga for in-situ XRD experiments, and Dr. Jinyong Luo for useful discussions and for help in setting up the NO_x storage capacity measurements. The research was performed in the Environmental Molecular Sciences Laboratory (EMSL), a national scientific user facility sponsored by the U.S. DOE's Office of Biological and Environmental Research, and located at Pacific Northwest National Laboratory (PNNL). PNNL is a multi-program national lab-oratory operated for the U.S. Department of Energy by Battelle.

References

- [1] N. Takahashi, H. Shinjoh, T. Iijima, T. Suzuki, K. Yamazaki, K. Yokota, H. Suzuki, N. Miyoshi, S. Matsumoto, T. Tanizawa, T. Tanaka, S. Tateishi, K. Kasahara, *Catal. Today* 27 (1996) 63.
- [2] N. Miyoshi, S. Matsumoto, K. Katoh, T. Tanaka, J. Harada, N. Takahashi, K. Yokota, M. Sugiura, K. Kasahara, SAE Technical Paper, 1995.
- [3] T.V. Johnson, *SAE Int. J. Engines* 4 (2011) 143.
- [4] http://delphi.com/manufacturers/auto/powertrain/emissions_standards/
- [5] W.S. Epling, L.E. Campbell, A. Yezerski, N.W. Currier, J.E. Parks, *Catal. Rev. Sci. Eng.* 46 (2004) 163.
- [6] S. Roy, A. Baiker, *Chem. Rev.* 109 (2009) 4054.
- [7] M.P. Harold, *Curr. Opin. Chem. Eng.* 1 (2012) 303.
- [8] T. Montanari, R. Matarrese, N. Artioli, G. Busca, *Appl. Catal. B: Environ.* 105 (2011) 15.
- [9] N. Takahashi, K. Yamazaki, H. Sobukawa, H. Shinjoh, *Appl. Catal. B: Environ.* 70 (2007) 198.
- [10] D.H. Kim, K. Mudiyanselage, J. Szanyi, H. Zhu, J.H. Kwak, C.H.F. Peden, *Catal. Today* 184 (2012) 2–7.
- [11] J. Luo, F. Gao, D.H. Kim, C.H.F. Peden, *Catal. Today* 231 (2014) 164.
- [12] T.J. Toops, D.B. Smith, W.P. Partridge, *Catal. Today* 114 (2006) 112.
- [13] D.H. Kim, K. Mudiyanselage, J. Szanyi, J.H. Kwak, H. Zhu, C.H.F. Peden, *Appl. Catal. B: Environ.* 142–143 (2013) 472.
- [14] L. Castoldi, R. Matarrese, L. Lietti, P. Forzatti, *Appl. Catal. B: Environ.* 90 (2009) 278.
- [15] R. Matarrese, L. Castoldi, N. Artioli, E. Finocchio, G. Busca, L. Lietti, *Appl. Catal. B: Environ.* 144 (2014) 783.
- [16] H. Imagawa, N. Takahashi, T. Tanaka, S.I. Matsunaga, H. Shinjoh, *Appl. Catal. B: Environ.* 92 (2009) 23.
- [17] H. Imagawa, T. Tanaka, N. Takahashi, S.I. Matsunaga, A. Suda, H. Shinjoh, *Appl. Catal. B: Environ.* 86 (2009) 63.
- [18] N. Takahashi, A. Suda, I. Hachisuka, M. Sugiura, H. Sobukawa, H. Shinjoh, *Appl. Catal. B: Environ.* 72 (2007) 187.
- [19] M. Takeuchi, S. Matsumoto, *Top. Catal.* 28 (2004) 151.
- [20] Q. Wang, J.H. Sohn, J.S. Chung, *Appl. Catal. B: Environ.* 89 (2009) 97.
- [21] Q. Wang, J.S. Chung, *Appl. Catal. A: Gen.* 358 (2009) 59.
- [22] W. Shen, A. Nitta, Z. Chen, T. Eda, A. Yoshida, S. Naito, *J. Catal.* 280 (2011) 161.
- [23] A. Yoshida, W. Shen, T. Eda, R. Watanabe, T. Ito, S. Naito, *Catal. Today* 184 (2012) 78.
- [24] Y. Zhang, M. Meng, F. Dai, T. Ding, R. You, *J. Phys. Chem. C* 117 (2013) 23691.
- [25] L. Li, F. Zhang, N. Guan, E. Schreier, M. Richter, *Catal. Commun.* 9 (2008) 1827.
- [26] Q. Wang, J.S. Chung, Z. Guo, *Ind. Eng. Chem. Res.* 50 (2011) 8384.
- [27] T. Zaremba, *J. Therm. Anal. Calorim.* 91 (2008) 911.
- [28] Z.Y. Yuan, X.B. Zhang, B.L. Su, *Appl. Phys. A-Mater. Sci. Process* 78 (2004) 1063.
- [29] X.M. Sun, X. Chen, Y.D. Li, *Inorg. Chem.* 41 (2002) 4996.
- [30] G.H. Du, Q. Chen, P.D. Han, Y. Yu, L.M. Peng, *Phys. Rev. B* 67 (2003).
- [31] L.M. Sikhwivihilu, S.S. Ray, N.J. Coville, *Appl. Phys. A-Mater. Sci. Process* 94 (2009) 963.
- [32] J. Szanyi, J.H. Kwak, D.H. Kim, X. Wang, R. Chimentao, J. Hanson, W.S. Epling, C.H.F. Peden, *J. Phys. Chem. C* 111 (2007) 4678.
- [33] I. Hachisuka, T. Yoshida, H. Ueno, N. Takahashi, A. Suda, M. Sugiura, SAE Technical Paper 2002-01-0732, 2002.
- [34] J.W. Xie, X.H. Lu, Y. Zhu, C. Liu, N.Z. Bao, X. Feng, *J. Mater. Sci.* 38 (2003) 3641–3646.
- [35] F. Prinetto, M. Manzoli, S. Morandi, F. Frola, G. Ghiootti, L. Castoldi, L. Lietti, P. Forzatti, *J. Phys. Chem. C* 114 (2010) 1127.
- [36] T. Montanari, L. Castoldi, L. Lietti, G. Busca, *Appl. Catal. A-Gen.* 400 (2011) 6.
- [37] T.J. Toops, D.B. Smith, W.S. Epling, J.E. Parks, W.P. Partridge, *Appl. Catal. B: Environ.* 58 (2005) 255.
- [38] J. Szanyi, J.H. Kwak, D.H. Kim, S.D. Burton, C.H.F. Peden, *J. Phys. Chem. B* 109 (2005) 27.
- [39] G.G. Ramis, G. Busca, V. Lorenzelli, P. Forzatti, *Appl. Catal.* 64 (1990) 243–257.
- [40] G.M. Underwood, T.M. Miller, V.H. Grassian, *J. Phys. Chem. A* 103 (1999) 6184.
- [41] M.A. Debeila, N.J. Coville, M.S. Scurrell, G.R. Hearne, *Appl. Catal. A: Gen.* 291 (2005) 98.
- [42] K. Hadjiivanov, V. Bushev, M. Kantcheva, D. Klissurski, *Langmuir* 10 (1994) 464.
- [43] K. Hadjiivanov, H. Knozinger, *Phys. Chem. Chem. Phys.* 2 (2000) 2803.